

**NOAA NESDIS
CENTER for SATELLITE APPLICATIONS and
RESEARCH**

ALGORITHM THEORETICAL BASIS DOCUMENT

Tropopause Folding Turbulence Product

Anthony Wimmers, Wayne Feltz UW/CIMSS

Version 2.0

May 10, 2010

TABLE OF CONTENTS

| | |
|---|----|
| LIST OF FIGURES | 4 |
| LIST OF TABLES | 6 |
| LIST OF ACRONYMS | 7 |
| ABSTRACT..... | 8 |
| 1.0 INTRODUCTION | 9 |
| 1.1 Who Should Use This Document | 9 |
| 1.2 Inside Each Section..... | 9 |
| 1.3 Related Documents | 9 |
| 1.4 Revision History | 10 |
| 2.0 OBSERVING SYSTEM OVERVIEW..... | 11 |
| 2.1 Products Generated | 11 |
| 2.2 Instrument Characteristics | 12 |
| 3.0 ALGORITHM DESCRIPTION..... | 13 |
| 3.1 Algorithm Overview | 13 |
| 3.2 Processing Outline | 14 |
| 3.3 Algorithm Input | 16 |
| 3.3.1 Primary Sensor Data | 16 |
| 3.3.2 Ancillary Data | 17 |
| 3.3.3 Derived Data | 17 |
| 3.4 Theoretical Description..... | 17 |
| 3.4.1 The Physics of the Problem | 17 |
| 3.4.2 Mathematical Description..... | 22 |
| 3.4.3 Algorithm Output..... | 29 |
| 4.0 TEST DATA SETS AND OUTPUTS | 32 |
| 4.1 Simulated Input Data Sets..... | 32 |
| 4.1.1 GOES-12 water vapor imagery..... | 32 |
| 4.1.2 GFS forecast model fields..... | 33 |
| 4.1.3 Test data set sample | 33 |
| 4.2 Output from Simulated Input Data Sets..... | 34 |
| 4.2.1 Precisions and Accuracy Estimates | 35 |
| 4.2.1.1 <i>Horizontal Precision</i> | 36 |
| 4.2.1.2 <i>Horizontal Accuracy</i> | 36 |
| 4.2.1.3 <i>Vertical Precision</i> | 36 |
| 4.2.1.4 <i>Vertical Accuracy</i> | 37 |
| 4.2.1.5 <i>Directional Precision</i> | 37 |
| 4.2.1.6 <i>Directional Accuracy</i> | 37 |
| 4.2.2 Error Budget..... | 37 |
| 5.0 PRACTICAL CONSIDERATIONS..... | 41 |
| 5.1 Numerical Computation Considerations | 41 |
| 5.2 Programming and Procedural Considerations | 41 |
| 5.3 Quality Assessment and Diagnostics | 42 |
| 5.4 Exception Handling | 42 |

| | |
|--|----|
| 5.5 Algorithm Validation | 42 |
| 5.5.1 Validation activities | 42 |
| 5.5.2 Independent validation data set..... | 42 |
| 5.5.3 Validation strategy | 43 |
| 5.5.3.1 <i>Rationale</i> | 43 |
| 5.5.3.2 <i>Applying an accuracy statistic on tropopause folds</i> | 43 |
| 5.5.3.3 <i>Normalizing the EDR observations to the appropriate scale</i> | 44 |
| 6.0 ASSUMPTIONS AND LIMITATIONS | 46 |
| 6.1 Performance | 46 |
| 6.2 Assumed Sensor Performance | 46 |
| 6.3 Pre-Planned Product Improvements | 46 |
| 6.3.1 Optimization for Ocean Domain..... | 46 |
| 6.3.2 Limitations of the Algorithm | 47 |
| 7.0 REFERENCES | 48 |

LIST OF FIGURES

| | |
|--|----|
| Figure 1. Example of Ridge and Reach features in the TFTP algorithm..... | 13 |
| Figure 2. High Level Flowchart of the TFTP illustrating the main processing sections. | 15 |
| Figure 3. Detailed Level Flowchart of the TFTP illustrating the main processing sections in expanded form. | 16 |
| Figure 4. Cross section through a tropopause folding event from Shapiro (1980). Potential temperature (K) thick solid lines; wind speed (m s^{-1}) heavy dashed lines; flight track, thin dashed lines; the $100 \times 100^{-7} \text{ K mb}^{-1} \text{ s}^{-1}$ potential vorticity tropopause, heavy solid line; troposphere, stippled area. | 18 |
| Figure 5. Frequency multiplied cospectra of vertical wind and ozone, and vertical wind and aerosol (CN) at a 366 mb transect (shown in Figure 4) for the top and bottom of the tropopause fold. Heavy arrows give the directions of the fluxes. From Shapiro (1980). | 19 |
| Figure 6. Idealized cross-section of a tropopause fold, with a projection of the distance- theta space in light gray. Blue and red lines are potential temperature contours..... | 20 |
| Figure 7. Frequency of Light or Greater (LOG) turbulence from EDR reports (December 2004 to February 2005) after applying all selective criteria. The white polygon delineates the region in which the TFTP predicts turbulence. Horizontal distance is Great Circle Degrees (1 GCD = ~ 111 km). | 21 |
| Figure 8. Left column: GOES-10 water vapor channel brightness temperature in color and grayscale; right column: GLASH product produced from this image, in color and grayscale..... | 22 |
| Figure 9. Cross section of a tropopause fold illustrating the difference in the retrieved upper-tropospheric water vapor levels from GLASH..... | 24 |
| Figure 10. a) GLASH product from a GOES-10 water vapor channel brightness temperature image, with a 232K threshold; b) A “smoothed” result of this image.. | 25 |
| Figure 11. a) Smoothed version of GLASH product; b) Gradient magnitude result, with a threshold of 3.2. | 26 |
| Figure 12. a) Gradient magnitude image; b) Contours of the laplacian zero-crossing (explained in text) to resolve major image boundaries..... | 26 |
| Figure 13. a) Contours from the previous figure; b) Processed tropopause folds that extend from the original contours into side of the warmer air mass, shown ovetop of the GLASH product. | 27 |
| Figure 14. Examples of flight direction relative to the tropopause fold. Left: Flight directions crossing tropopause folds at 20° . Right: Flight directions crossing at 110° . The black arrows are the orientations of the tropopause folds. The “caution directions” of the larger and smaller tropopause folds are perpendicular to the black arrow: 315° , 135° for the larger; and 0° , 180° for the smaller (yellow vectors). | 28 |
| Figure 15. Height assignment of the tropopause folds..... | 29 |
| Figure 16. Cross-sectional depiction of the tropopause fold height assignment. | 29 |
| Figure 17. Domain of the input data sets, using GOES-12 water vapor archived imagery. This example is for 6 April 2006 2345 UTC. | 33 |
| Figure 18. GLASH product corresponding to the previous figure to show the input domain in the rectilinear coordinates used in subsequent figures..... | 33 |

| | |
|--|----|
| Figure 19. TFTP output products for 6 April 2006 2345 UTC. Upper-left: Fold lower height (kft); Upper-right: Fold upper height (kft), Lower-left: Caution direction #1 (degrees); Lower-right: Caution direction #2 (degrees). | 35 |
| Figure 20. In-situ validation data for 6 April 2006 2315 UTC; MOG turbulence observations are “hot” colors – yellow, orange and red; light turbulence is green and null values are gray. Top: Horizontal distribution; bottom: Vertical distribution. ... | 38 |
| Figure 21. As in Figure 17, but limited to the volume and direction of the predicted tropopause folds. | 39 |
| Figure 22. Conceptual diagram of two aircraft passes through a tropopause fold, scaled to the average width of a tropopause fold (shown in gray) and the typical speed of a commercial jet passing through. Areas of short-lived atmospheric instability are shown in yellow. Green segments are “no turbulence” reports and red segments are turbulent reports. The top pass supposes a one-minute interval between observations, and the bottom pass supposes a 16-minute interval between observations. | 44 |

LIST OF TABLES

| | |
|--|----|
| Table 1. Product Requirements. | 11 |
| Table 2. Adjustments to modify and filter tropopause fold objects. | 27 |
| Table 3. TFTP output products. | 29 |
| Table 4. TFTP Metadata output. | 30 |
| Table 5. Times of the sample images for the initial verification..... | 33 |
| Table 6. Summary of the sources of output precision and accuracy..... | 36 |
| Table 7. Results of the most recent TFTP validation..... | 40 |

LIST OF ACRONYMS

| | |
|--------|--|
| ABI | Advanced Baseline Imager |
| AIT | Algorithm Integration Team |
| ATBD | Algorithm Theoretical Basis Document |
| AWG | Algorithm Working Group |
| CIMSS | Cooperative Institute for Meteorological Satellite Studies |
| CN | Condensation Nuclei |
| CONUS | Continental United States (satellite scanning domain) |
| ECMWF | European Centre for Medium-range Weather Forecasts |
| EDR | Eddy Dissipation Rate |
| F&PS | Functional and Performance Specification |
| GFS | Global Forecast System (model) |
| GLASH | GOES Layer Average Specific Humidity |
| GOES | Geostationary Operational Environmental Satellite |
| GS | Ground Segment |
| LZA | Local Zenith Angle |
| LOG | Light or Greater (turbulence) |
| McIDAS | Man-Computer Interactive Data Access System |
| MOG | Moderate or Greater (turbulence) |
| MRD | Mission Requirements Document |
| NASA | National Aeronautics and Space Administration |
| NCAR | National Center for Atmospheric Research |
| NetCDF | Network Common Data Form |
| NOAA | National Oceanic and Atmospheric Administration |
| NWP | Numerical Weather Prediction (model) |
| RH | Relative Humidity |
| TFTP | Tropopause Fold Turbulence Product |
| TKE | Total Kinetic Energy |
| UW | University of Wisconsin |
| VAGL | Vendor-Allocated Ground Latency |
| WMO | World Meteorological Organization |

ABSTRACT

At the upper-tropospheric boundary between air masses, the vertical shearing at the jet stream combined with the ageostrophic convergence of polar, subtropical and stratospheric air produces a region known for its potential for clear air turbulence called a “tropopause fold.” These features are evident in satellite-observed upper tropospheric water vapor by the large-scale spatial gradients in brightness temperature, which define boundaries between the air masses. The tropopause fold extends from this boundary to a limited distance into and underneath the wetter air mass.

The Tropopause Folding Turbulence Prediction (TFTP) product is designed to locate these regions in the atmosphere and identify the sections most likely to produce turbulent flight conditions for aircraft. The upper-tropospheric water vapor channel of the GOES-R Advanced Baseline Imager (channel 8) is the source for resolving gradients that reveal the horizontal distribution of tropopause folds. An ancillary numerical weather model constrains these features vertically in the atmosphere. The four key output products consist of two fields that define the lower and upper bounds of the tropopause fold features, and two fields that define the two flight directions that are the most susceptible to moderate or greater turbulence.

This document lays out a high-level description of the algorithm: the procedural flow; the characteristics of the input/output; a detailed theoretical description; an account of test data sets, validation data and algorithm performance with pre-launch input/output examples; practical considerations; and assumptions and limitations of the algorithm.

1.0 INTRODUCTION

This algorithm theoretical basis document (ATBD) provides a high level description of and the physical basis for the detection of volumes of dynamical instability due to tropopause folding leading to aircraft turbulence. The algorithm uses images from the Advanced Baseline Imager (ABI) flown on the GOES-R series of NOAA geostationary meteorological satellites. This is an end-product with no dependent ABI products.

1.1 Who Should Use This Document

The intended users of this document are those interested in understanding the physical basis of the algorithms and how to use the output of this algorithm to optimize the turbulence detection for a particular application. This document also provides information useful to anyone maintaining or modifying the original algorithm.

1.2 Inside Each Section

This document is broken down into the following main sections.

- **2.0 Observing System Overview:** Provides relevant details of the ABI and provides a brief description of the products generated by the algorithm.
- **3.0 Algorithm Description:** Provides the detailed description of the algorithm including its physical basis, its input and its output.
- **4.0 Test Data Sets and Outputs:** Describes the forms of input data set to test the algorithm pre-launch and characterizes the output data.
- **5.0 Practical Considerations:** Presents the relevant issues involving numerical computation, programming and procedures, quality assessment/diagnostics and exception handling.
- **6.0 Assumptions and Limitations:** Provides an overview of the current limitations of the approach and gives the plan for overcoming these limitations with further algorithm development.

1.3 Related Documents

This document currently does not relate to any other document outside of the specifications of the Mission Requirements Document (MRD) and to the references given throughout.

1.4 Revision History

Version 0.1 of this document was created by Dr. Anthony Wimmers and Mr. Wayne Feltz of UW/CIMSS to accompany the delivery of the version 0.1 algorithm to the GOES-R AWG Algorithm Integration Team (AIT).

Version 2.0 is written to meet the 80% delivery requirement due to the AIT in May 2010.

Version 2.1 addresses comments from outside reviewers and documents QC variable inclusions

2.0 OBSERVING SYSTEM OVERVIEW

2.1 Products Generated

The TFTP algorithm calculates volumes of the atmosphere where turbulence due to tropopause folding is more likely to be experienced by aircraft. It also calculates the directions of flight in which turbulence is expected. It *does not* provide a complete account of all volumes of the atmosphere prone to turbulence due to other factors such as mountain waves or convection.

The volume of atmosphere containing tropopause folds is constrained by the first two output fields – Lowermost height and Uppermost height. (Regions without tropopause folds, which constitute the majority of pixels of any output field, are marked with missing values.) The second two output fields describe the directions of flight prone to turbulence – “Caution directions” #1 and #2. The output products meet the algorithm product requirements listed in Table 1.

Table 1. Product Requirements.

| | Threshold | |
|---|---|-----------|
| Geographic Coverage | Full Disk | Mesoscale |
| User & Priority | GOES-R | |
| Vertical Resolution | Sfc – 100mb | |
| Horizontal Resolution | 2 km | |
| Mapping Accuracy | 1 km | |
| Measurement Range | Binary yes/no detection above boundary layer for Moderate or Greater (MOG) turbulence | |
| Measurement Accuracy | 50% or greater detection of MOG turbulence | |
| Product Refresh Rate/Coverage (Mode 3) | 15 min | 5 min |
| Product Refresh Rate/Coverage (Mode 4) | 5 min | 5 min |
| Vendor Allocated Ground Latency | 159 sec | |
| Product Measurement Precision | N/A | |
| Temporal Coverage Qualifier | Day and night | |
| Product Extent Qualifier | Quantitative out to at least 70 degrees LZA and qualitative at larger LZA | |
| Cloud Cover Condition Qualifier | Clear conditions down to feature of interest associated with threshold accuracy | |
| Product Statistics Qualifier | Over the lengths of separate flight transects through the region of positive prediction | |

The turbulence observation requirements are summarized based on the GOES-R Series Ground Segment (GS) Functional and Performance Specification (F&PS) (NOAA/NASA 2008).

2.2 Instrument Characteristics

The TFTP uses the following channel set from the ABI:

- Calibrated brightness temperature from channel 8 (6.15 μm)

The TFTP product images are produced at the temporal and spatial resolution of the ABI. Currently this equates to one CONUS product every 5 minutes and one Full Disk product every 15 minutes. The spatial resolution is 2 km and the mapping accuracy is 1 km.

Because the TFTP relies heavily on the computation of gradients in a water vapor channel of the ABI, it is highly sensitive to scanline noise. It is comparatively insensitive to more random noise, such as thermal noise, because it uses a spatial filter (~66 km wide) to smooth out such distortions. A quality flag that indicates the output pixels affected by scanline noise is still in development.

The TFTP algorithm can be easily adapted to work with any satellite's upper tropospheric water vapor channel because the gradient signatures are so similar between various wavelength bands sensitive to upper tropospheric water vapor. Calibration/validation is performed with GOES-12 channel 3 (water vapor) (Sections 4.2 and 5.5).

3.0 ALGORITHM DESCRIPTION

The following is a complete description of the algorithm at the current level of maturity.

3.1 Algorithm Overview

The tropopause folding turbulence product (TFTP) is designed to resolve volumes of dynamical turbulence caused by tropopause folds at air mass boundaries. Tropopause folds are located by their association with gradients in moisture, which are evident in a band in the ABI sensitive to upper tropospheric water vapor.

This routine uses the ABI 6.1 μm water vapor channel to infer the presence of tropopause folds in the midtroposphere and upper troposphere. It first calculates the GOES Layer Average Specific Humidity (GLASH) product from the water vapor channel and model temperature fields. Large-scale gradients in specific humidity indicate tropopause breaks, and the routine designates a ~ 222 km-wide tropopause fold extending from the tropopause break boundary. The inner edge of the tropopause fold extending from the tropopause break is named the "ridge" (after "ridges" in the gradient field) and the side that is the outer edge is named the "reach" (Figure 1).

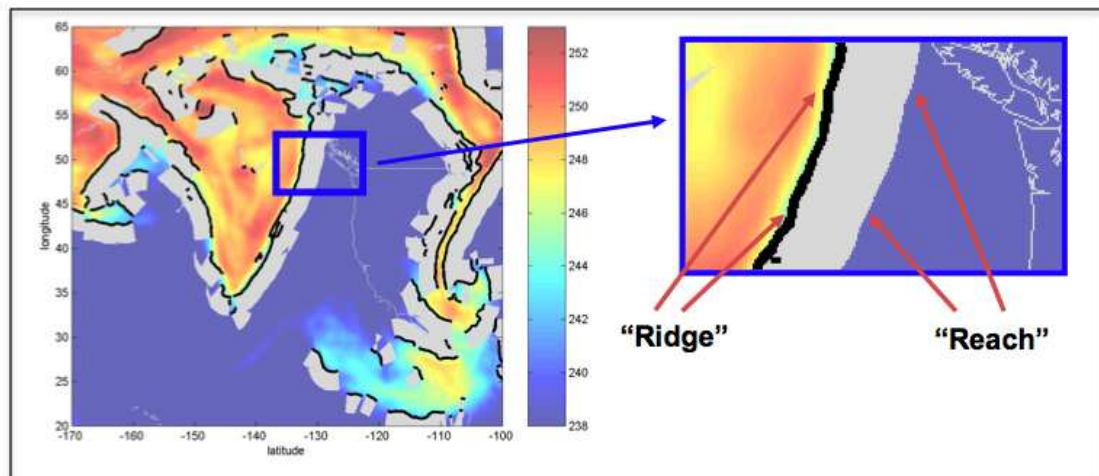


Figure 1. Example of Ridge and Reach features in the TFTP algorithm.

The height of the tropopause fold "ridge" is the height of the lowest thermal tropopause in the vicinity (because a tropopause fold extends down from the tropopause of the colder side). The height of the "reach" is the height of the isentropic surface 5K below the potential temperature of the "ridge." The range of heights that bound the tropopause fold volume is based on these two heights of the edges.

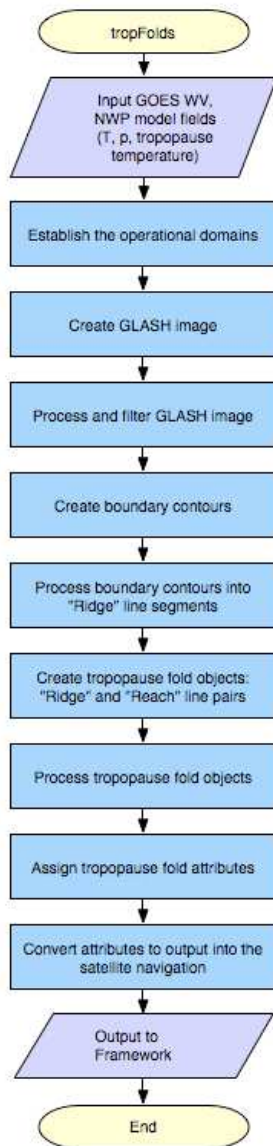
The orientation of the tropopause fold is used to infer the orientation of turbulent eddy axes. The most common way for an aircraft to experience turbulence is for the flight path to be oriented perpendicularly with the eddy axis. Therefore this routine also outputs the range of flight directions that are the most likely to experience turbulence.

In its current application to identify areas of aircraft turbulence due to tropopause folding with the highest possible accuracy, we produce the following product fields:

- Lowermost height of the distribution of regions prone to turbulence
- Uppermost height of the distribution of regions prone to turbulence
- Range of directions in which a flight pattern is prone to turbulence within the given regions because turbulence is direction-sensitive (two fields for each opposing direction)

3.2 Processing Outline

The processing outline of the TFTP is summarized in Figures 2 and 3 below. The current TFTP is implemented within the GOES-R AWG Framework. The Framework provides the input imagery and ancillary NWP fields. Unlike most of the other products that are part of the framework, the TFTP operates on very large segments of data in a single iteration. Most products process a few scan lines at a time. However, the TFTP processes the entire image at once for a northern hemisphere image, and processes a full disk image as two segments (the northern and southern halves.)



| | | | | |
|--|-----------|-----------|-------------|--------|
|  Space Science & Engineering Center University of Wisconsin - Madison 1225 W. Dayton St. Madison, WI, 53706 | | | | |
| Title: Overview flowchart: tropFolds | | | | |
| Drawing Number: | | Revision: | | |
| Project Number: | Research: | Date: | Created by: | Page: |
| | | 3/2010 | AJW | 1 of 1 |

Input Data:
GOES-12 or simulated ABI

Imager channels used:
3 (GOES-12), 9 (ABI)

Algorithm Dependencies:
None

Ancillary Data Dependencies:
NWP: 0.5 to 1 degree temperature, pressure heights, tropopause height (if available)

Products Generated:
Tropopause fold distribution
Tropopause fold lower height
Tropopause fold upper height
Hazardous flight direction #1
Hazardous flight direction #2

Figure 2. High Level Flowchart of the TFTP illustrating the main processing sections.

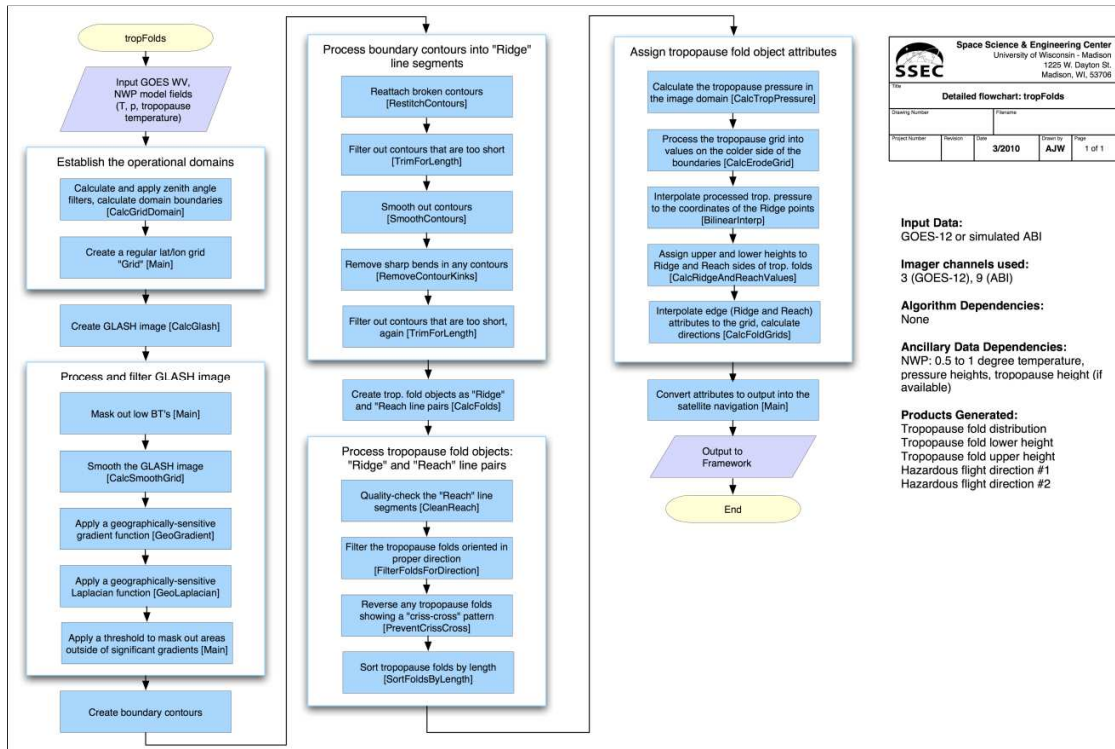


Figure 3. Detailed Level Flowchart of the TFTP illustrating the main processing sections in expanded form.

3.3 Algorithm Input

This section describes the input needed to process the TFTP.

3.3.1 Primary Sensor Data

The item below describes the primary sensor data used by the TFTP. By primary sensor data, we mean information that is derived solely from the ABI observations and geolocation information.

- Calibrated brightness temperature for channel 8 (6.15 μm , water vapor)

The product cannot be generated without data from this channel. However, because of the heavy use of spatial averaging in this channel, the product quality is not degraded with any uniform brightness temperature bias or thermal noise less than 4 K. Scan line noise would pose a significant problem, and this possibility will be handled in a future release with scan line noise quality flags.

3.3.2 Ancillary Data

The following items list and briefly describe the ancillary data required to run the TFTP. By “ancillary data,” we mean data that requires information not included in the ABI observations or geolocation data.

- **Global forecast system (GFS) model temperature and pressure fields**
Model temperature fields are used in creating the GLASH image, because temperature fields are necessary to adjust the water vapor image of brightness temperature to vary only according to moisture. Temperature fields at any given time are interpolated from available fields at 6-hour temporal resolution. Only levels 300, 400 and 500 hPa are used. In addition, temperature and pressure fields at all levels are used to compute the tropopause height if it is not included in the model fields
- **Global forecast system (GFS) model tropopause height fields**
Model-derived tropopause heights are necessary for the vertical assignment of tropopause fold regions.

3.3.3 Derived Data

The GLASH product is derived internally (Section 3.4.2). When a tropopause height is not included in the ancillary model fields, it is also derived internally.

3.4 Theoretical Description

This section describes the physical processes and features that the derived product seeks to estimate, the methods used to locate those features and the output products that constrain these features in space.

3.4.1 The Physics of the Problem

Our algorithm focuses on turbulence in upper-tropospheric frontal systems, which have been investigated for decades as a dynamically active and varied atmospheric phenomenon. A natural first step toward understanding the physics of the problem may seem to be a characterization of some indicator of turbulence similar to the Reynolds number in a mathematically simplified case of an upper-level front. However, a definitive mathematical indicator of atmospheric turbulence does not exist. Even in controlled laboratory experiments, the Reynolds number of a fluid is only a general guide as to the tendency of the fluid to change from laminar to turbulent flow, or to indicate the strength and spatial scale of ongoing turbulence. The development of eddies that receive energy from the background flow and deliver it to smaller and smaller physical scales is part of the chaotic and stochastic properties of fluid flow, severely limiting its predictability.

The turbulence with which we are concerned is the appropriate scale of eddy activity whose effects are experienced by aircraft. This can be approached by way of the larger

mechanisms that cause the phenomenon; however, these mechanisms are still generally understood and communicated either descriptively or on a case-by-case basis with atmospheric models. In either approach, one must still bridge the gap between theory and observation with empirical relationships. Thus, our best method for presenting the physics of the problem as follows is to briefly summarize the science of upper-tropospheric fronts, explain the sources of turbulent flow in these fronts descriptively and connect this activity empirically to the experience of aircraft turbulence.

A mature characterization of upper-air fronts was not possible until intensive flight campaigns in the 1960s and 1970s, and the modern theory of fronts, the jet stream and the tropopause developed in tandem with the interpretation of aircraft data collected from these campaigns (Shapiro and Keyser, 1990). A key element of the upper-air front is the tropopause fold (Figure 4), which is a “tongue” of stratospheric air drawn into the air mass boundary by ageostrophic forcing (Keyser et al., 1986; Holton et al., 1995). In the figure below, the dominant component of the wind velocity is directed out of the page, which is consistent with the geostrophic flow. However, in the theory of extratropical cyclonic development, the orthogonal ageostrophic wind flows roughly parallel to the windspeed contours in this cross-section, and clockwise. This acts to deform and intensify, or in other words “sharpen” the air mass boundary and draw stratospheric air into this transitional region (Keyser and Pecnick, 1985a,b; Reeder and Keyser, 1988). The evidence of the stratospheric influence of this boundary is the concentrations of ozone, aerosol and especially the elevated potential vorticity (Danielson, 1968).

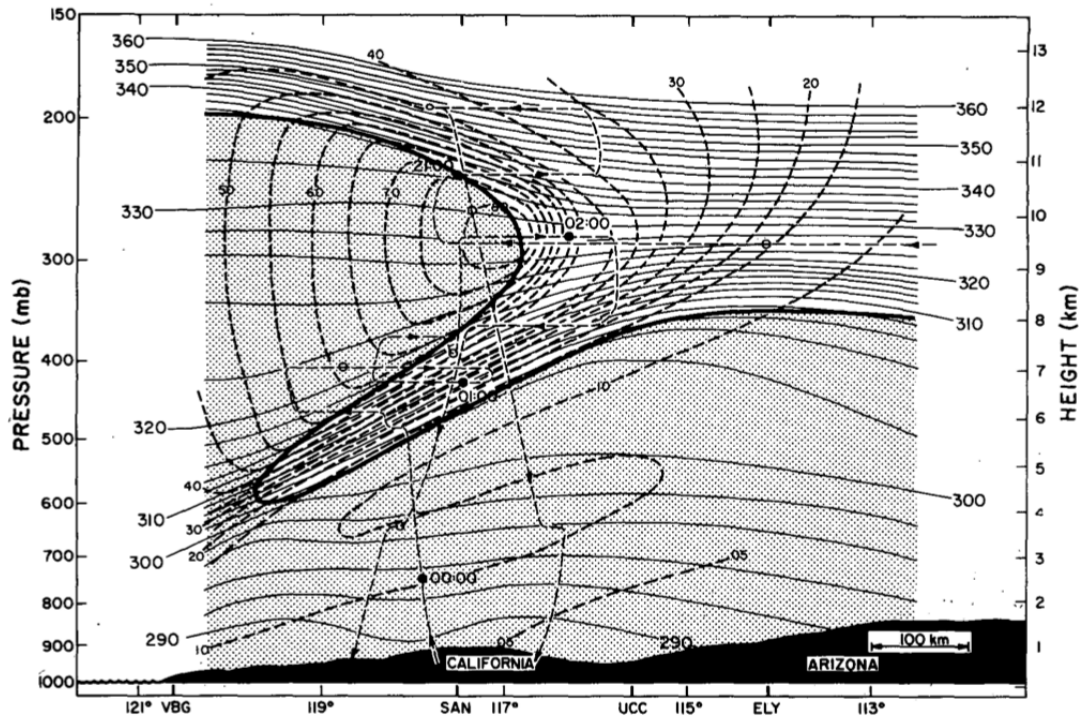


Figure 4. Cross section through a tropopause folding event from Shapiro (1980). Potential temperature (K) thick solid lines; wind speed ($m s^{-1}$) heavy dashed lines; flight

track, thin dashed lines; the $100 \times 100^{-7} \text{ K mb}^{-1} \text{ s}^{-1}$ potential vorticity tropopause, heavy solid line; troposphere, stippled area.

In the typical upper-air front this tongue of stratospheric air is delineated by a clear gradient in potential vorticity at its boundary. Potential vorticity is a convenient conservative tracer for stratospheric air, but its boundaries are also indicative of the location of vertical shear, which can lead to turbulence.

The interior of the tropopause fold is thermally stable but highly vertically sheared. However, the upper and lower boundaries of the tropopause fold are similarly sheared but lacking in the same thermal stability, making these regions more prone to turbulence. Indeed, Shapiro (1981) derives the dynamics showing that this turbulence is necessary for maintaining the high momentum gradients across the front.

To underscore this point, Shapiro (1980) presented the evidence for intense mixing across the boundary of the tropopause fold: a flux of ozone (stratospheric origin) outside of the tropopause fold and a flux of aerosol (tropospheric origin) into the tropopause fold (Figure 5). Chemical mixing of this type has since been confirmed in other aircraft campaigns (e.g. Johnson and Viezee, 1981; Cho et al., 1999) and with lidar observations (e.g. Browell et al., 2003).

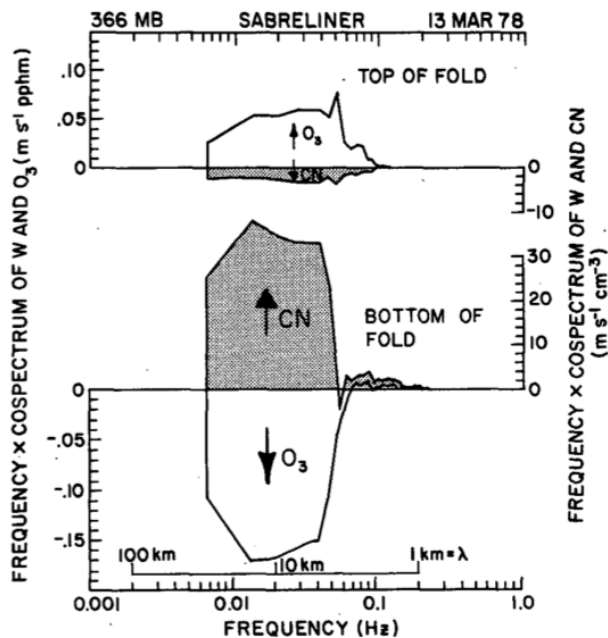


Figure 5. Frequency multiplied cospectra of vertical wind and ozone, and vertical wind and aerosol (CN) at a 366 mb transect (shown in Figure 4) for the top and bottom of the tropopause fold. Heavy arrows give the directions of the fluxes. From Shapiro (1980).

The vertical shearing and lower thermal stratification in the upper and lower boundaries of the tropopause fold (highlighted in an idealized model in Figure 6) generate favorable instability metrics that bear some relationship to the experience of turbulence, such as the gradient Richardson number (where a lower value indicates more instability)

$$Ri = \frac{\frac{g}{T_v} \frac{\partial \theta}{\partial z}}{\left(\frac{\partial U}{\partial z}\right)^2 + \left(\frac{\partial V}{\partial z}\right)^2}, \quad (1)$$

or the Diagnostic TKE function (DTF3, where higher values indicate more instability) (Marroquin 1998)

€

$$\varepsilon = K_M \left[\frac{c_1}{c_2} \left(\left(\frac{\partial U}{\partial z} \right)^2 + \left(\frac{\partial V}{\partial z} \right)^2 \right) - \frac{c_2}{c_3} \frac{\left(\frac{g}{T_v} \frac{\partial \theta}{\partial z} \right)}{Pr} \right] \quad (2)$$

where c_1 , c_2 and c_3 are fixed; and K_M and Pr are adjustable constants.

€

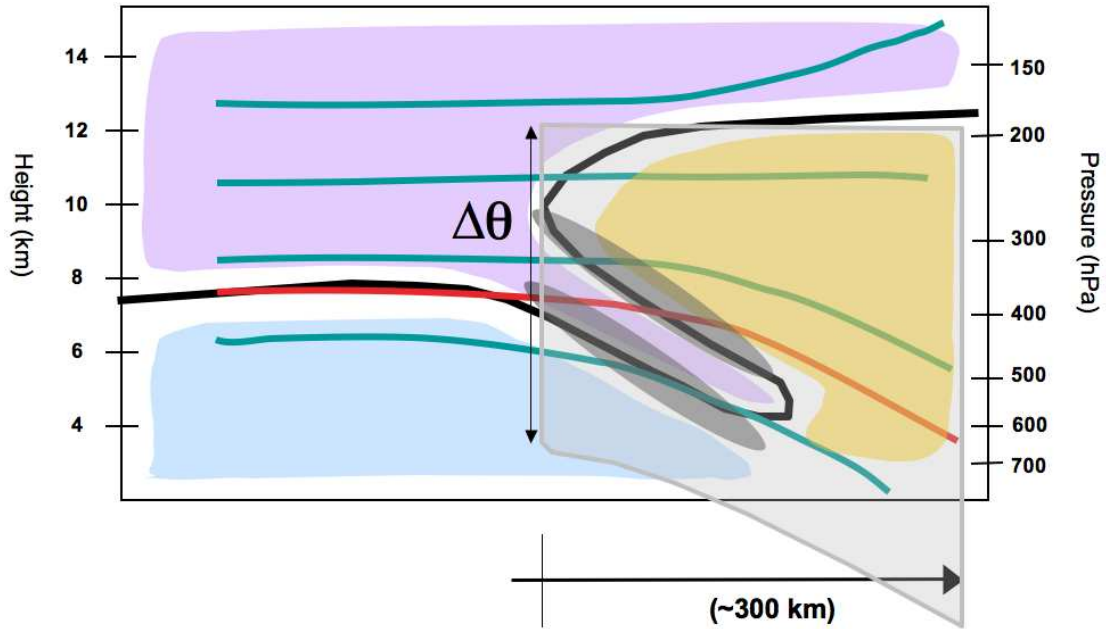


Figure 6. Idealized cross-section of a tropopause fold, with a projection of the distance-theta space in light gray. Blue and red lines are potential temperature contours.

When estimating the location of tropopause folds from satellite observations, the slant of the frontal boundary, its width and its vertical displacement are not known with enough precision to distinguish the upper and lower boundary. Thus, the region of interest in the vertical cross section becomes the entire tongue of the tropopause fold. In the projection of the tropopause fold cross-section into distance-theta space, this region of interest is a thicker, single slab, slanting into lower potential temperatures with distance from the opening, or “break,” of the tropopause fold (Figure 7).

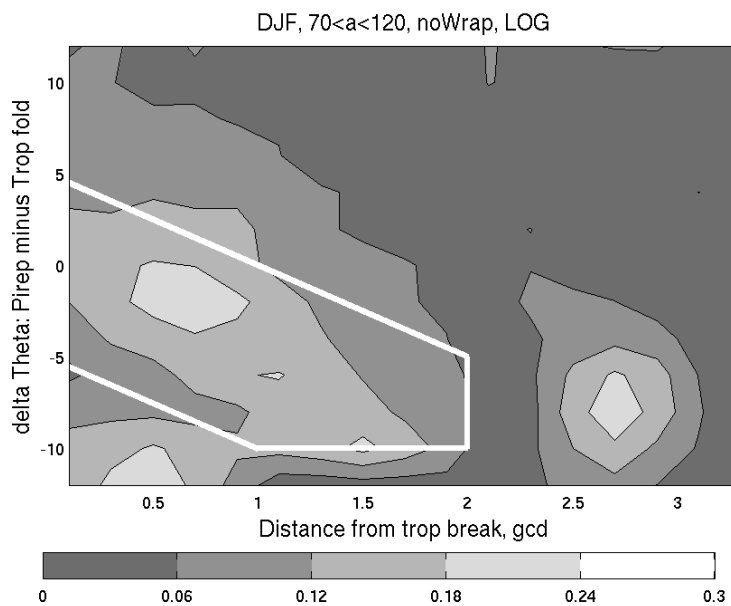


Figure 7. Frequency of Light or Greater (LOG) turbulence from EDR reports (December 2004 to February 2005) after applying all selective criteria. The white polygon delineates the region in which the TFTP predicts turbulence. Horizontal distance is Great Circle Degrees (1 GCD = ~111 km).

The above figure is the compilation from a previous 3-month validation using Light or Greater (LOG) turbulence automated observations, showing that LOG turbulence occurs at the scale of commercial aircraft speeds and sizes with impressive frequency in the vicinity of tropopause folds (a frequency of 20% in each minute of flight) (Wimmers and Feltz, 2005). A more thorough validation that addresses the TFTP product requirements is presented in Section 4.2.

3.4.2 Mathematical Description

The TFTP algorithm processes images from the upper-tropospheric water vapor channel to resolve their most prominent upper air mass boundaries and then project the presence of tropopause folds out from those boundaries. Unlike many other GOES-R algorithms, it does not retrieve atmospheric properties within single pixels individually. Rather, it operates on synoptic-scale grids of pixels and derives geometric shapes and volumes from the data.

First, the algorithm calculates a derived product called the GOES Layer-Average Specific Humidity (GLASH). The GLASH product is the operand for the subsequent edge-detection operations, because it resolves air mass boundaries more effectively than the original water vapor channel brightness temperatures (Figure 8).

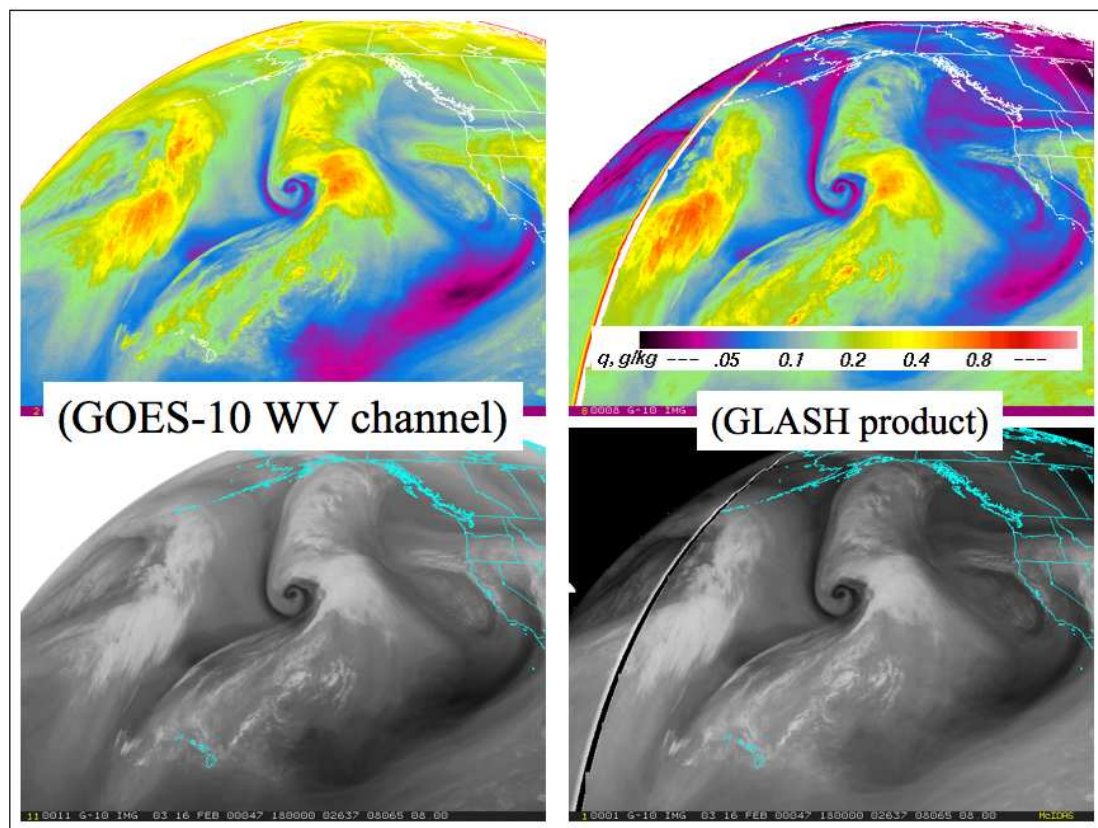


Figure 8. Left column: GOES-10 water vapor channel brightness temperature in color and grayscale; right column: GLASH product produced from this image, in color and grayscale.

The mathematical basis for the GLASH product is as follows. Soden and Bretherton (1996) approximated the water vapor channel brightness temperature ($T_{6.7}$) as a function of upper tropospheric relative humidity:

$$\log\left(\frac{RH}{\cos\theta}\right) = a - b \cdot T_{6.7}, \quad \text{or} \quad (3)$$

$$\log(RH) - \log(\cos\theta) = a - b \cdot T_{6.7}$$

where θ is the satellite zenith angle and (a, b) are constants. According to the derivation in Wimmers and Moody (2003), the relative humidity term can be further separated into specific humidity and an ancillary upper-tropospheric temperature field by the Clausius-Clapeyron relationship:

$$\log(RH) = \log(q) - c_1 \bar{T} + c_0, \quad (4a)$$

where \bar{T} is the weighted average of upper-tropospheric temperature:

$$\bar{T} = 0.25T_{300} + 0.50T_{400} + 0.25T_{500} \quad (4b)$$

and where T_{300} indicates the temperature at 300 hPa, and so on. Combining Equations (3) and (4) produces the GLASH product:

$$GLASH = c_q \log(q) + c_{q0} = T_{6.7} - \bar{T} - c_\theta \log(\cos\theta) + c. \quad (5)$$

The GLASH product isolates the specific humidity variance in the satellite signal, which is a quasi-conservative atmospheric tracer that allows a very easy identification (and quantification) of air mass moisture and air mass boundaries. In our algorithm's calculation of the GLASH product,

$$GLASH = T_{6.7} - \bar{T} - 8.90K \cdot \log(\cos\theta) + 240K. \quad (6)$$

Air mass boundaries are readily identified by their gradients of specific humidity, which are the greatest in the upper troposphere at breaks in the tropopause height (Figure 9).

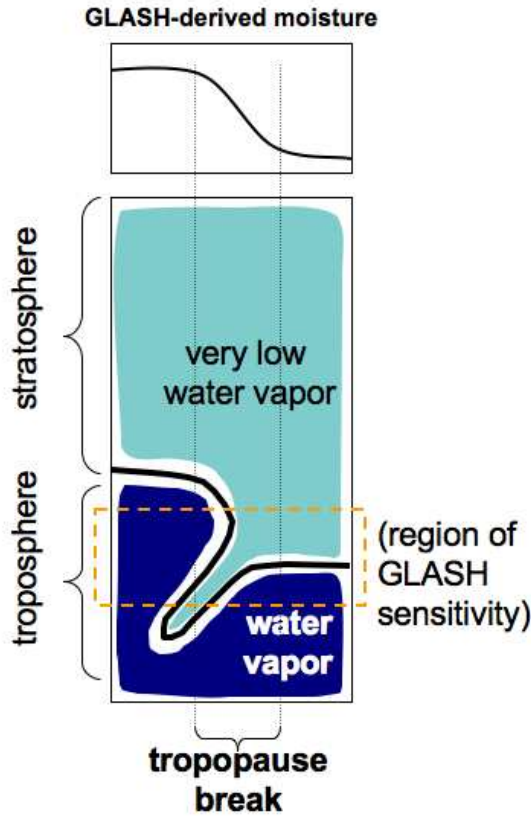


Figure 9. Cross section of a tropopause fold illustrating the difference in the retrieved upper-tropospheric water vapor levels from GLASH.

To show how the GLASH product is processed to retrieve these boundaries, we move from the vertical transect frame of reference used in the several previous figures to the horizontal satellite image domain.

Beginning with the GLASH image we apply a coarse but effective cloud-clearing formula:

$$GLASH(GLASH < 232K) = 232K. \quad (7)$$

The image is then smoothed (“blurred”) with a Gaussian smoothing parameter $\sigma = 0.30$ degrees (33 km, meaning a smoothing kernel diameter of ~66 km).

$$GLASH(smoothed) =$$

$$G_{\sigma} * I(\phi_0, \theta_0) = \sum_{i=i_0-N}^{i_0+N} \sum_{j=j_0-M}^{j_0+M} w(\phi_{i_0}, \theta_{j_0}, \phi_i, \theta_j, \sigma) I(\phi_i, \theta_j), \quad (8a)$$

where

$$w_{gc}(\phi_{i0}, \theta_{j0}, \phi_i, \theta_j, \sigma) = c \cdot \exp\left(-\frac{(\phi_i - \phi_{i0})^2}{2(\sigma \sec \theta_j)^2} - \frac{(\theta_j - \theta_{j0})^2}{2\sigma^2}\right) \quad (8b)$$

and

$$c = \left[\sum_{i=i0-N}^{i0+N} \sum_{j=j0-M}^{j0+M} w_{gc}(\phi_{i0}, \theta_{j0}, \phi_i, \theta_j, \sigma) \right]^{-1}; \quad (8c)$$

where I is the input image, (ϕ, θ) are the longitude and latitude, and (ϕ_0, θ_0) is the point being operated on.

The resulting output grid is shown in Figure 10.

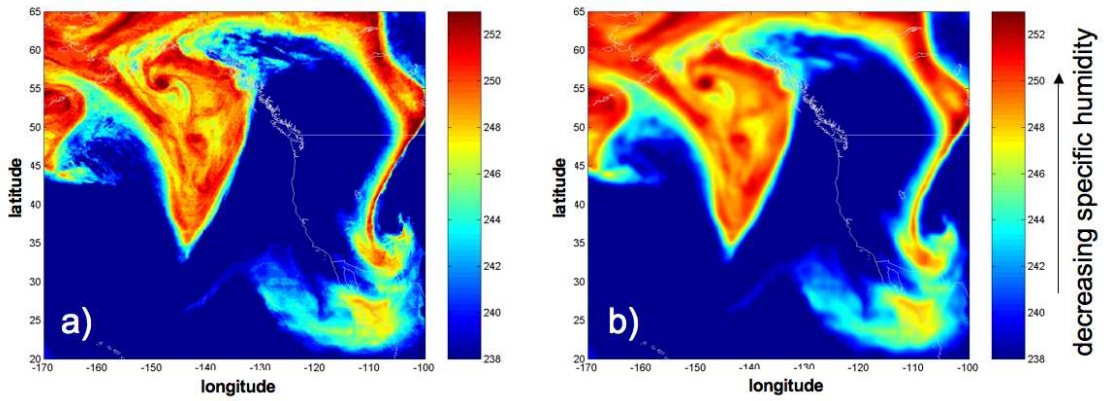


Figure 10. a) GLASH product from a GOES-10 water vapor channel brightness temperature image, with a 232K threshold; b) A “smoothed” result of this image.

A simple gradient magnitude function allows a quantitative view of the major boundaries (Figure 11).

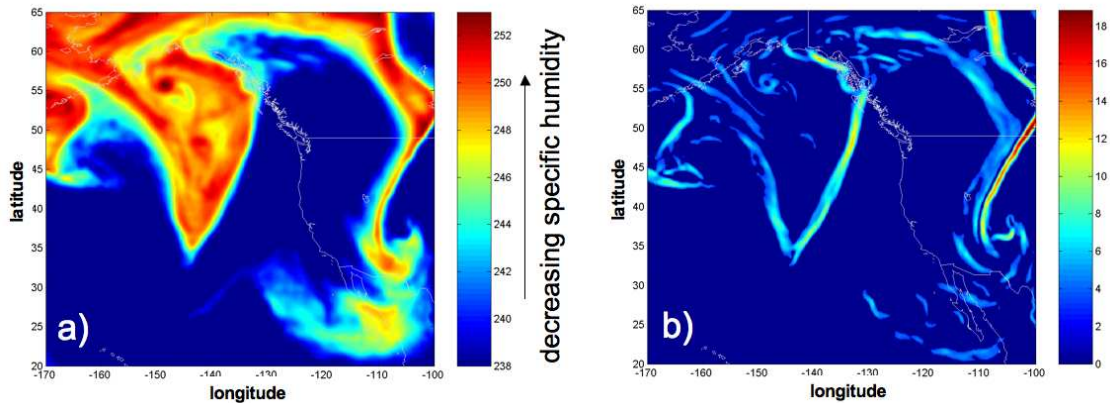


Figure 11. a) Smoothed version of GLASH product; b) Gradient magnitude result, with a threshold of 3.2.

Next, a contour along the value

$$\nabla^2 I = 0 \tag{9}$$

draws line segments along the image boundaries. In this formula, I is the input image (the smoothed GLASH image), and the laplacian operator is adjusted for geographic dimensions. In the parlance of digital image processing this is the “Laplacian zero-crossing.”

Only the line segments inside a gradient magnitude threshold of 3.2 K deg^{-1} are kept (Figure 12).

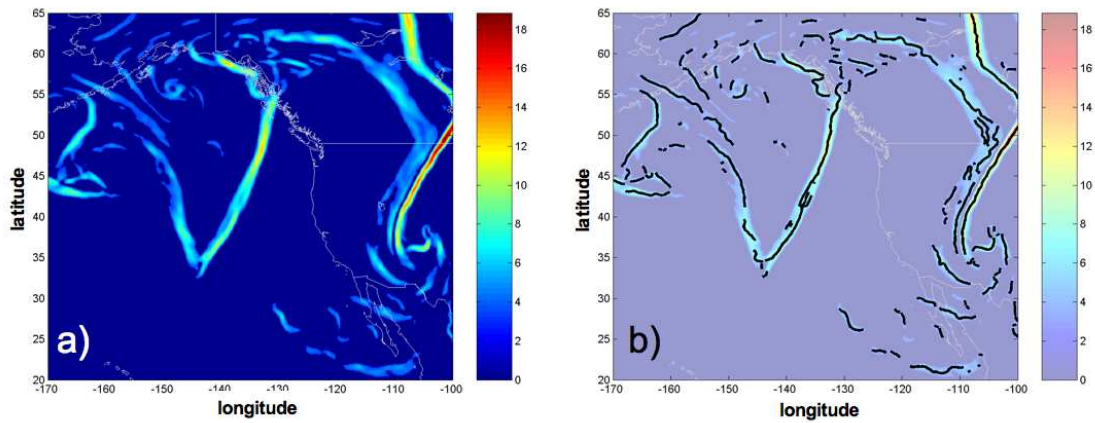


Figure 12. a) Gradient magnitude image; b) Contours of the laplacian zero-crossing (explained in text) to resolve major image boundaries.

In order to produce physically-based estimates of tropopause fold locations from these line segments, the boundaries from Figure 10b are used as one side of a tropopause fold anchored to the tropopause break. The opposite side of the tropopause fold, reaching out into the troposphere, is positioned 2 degrees (222 km) out and toward the higher humidity side of the tropopause break (Figure 11). The space between these two sides defines a polygon (in gray) of the horizontal distribution of the tropopause fold (Wimmers and Moody, 2004a,b). In the algorithm code, these two line segments that make up the two sides of the tropopause fold are named the “ridge” and the “reach.”

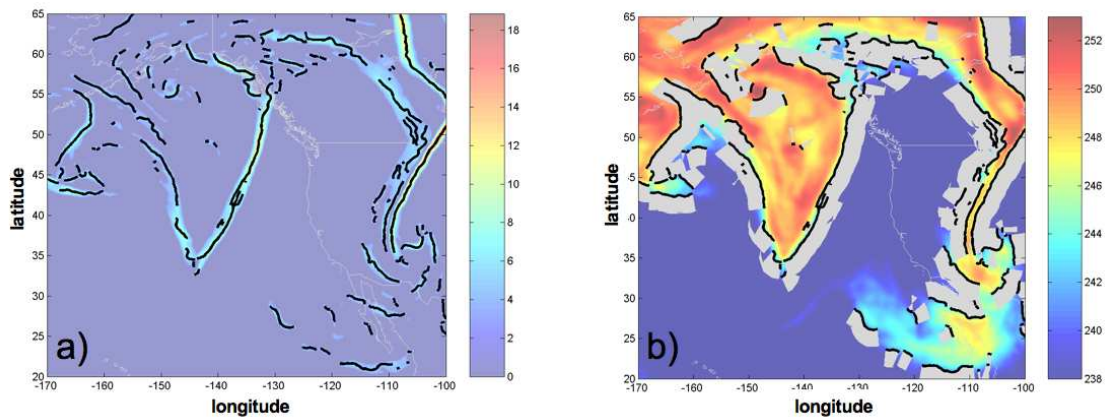


Figure 13. a) Contours from the previous figure; b) Processed tropopause folds that extend from the original contours into side of the warmer air mass, shown overtop of the GLASH product.

The folds in this figure mark the areas expected to have stratospherically-enhanced air at the air mass boundaries. However, only an especially dynamically active subset of these tropopause folds is associated with turbulence. Therefore a number of filtering criteria are applied to that initial set the tropopause folds in order to identify the turbulent tropopause folds only. These criteria are summarized in Table 2.

Table 2. Adjustments to modify and filter tropopause fold objects.

| Process | Function | Importance |
|---|----------|------------|
| 1. Eliminate fold objects less than a specific length (2 degrees) | Filter | High |
| 2. Smooth edges with an averaging filter | Modify | Medium |
| 3. Remove sharp twists in object edges | Repair | Medium |
| 4. Repeat filter for object length | Filter | Medium |
| 5. Prevent inward-curling edges in the outward-reaching side | Modify | High |
| 6. Eliminate tropopause fold objects aligned in directions that do not normally show turbulence | Filter | High |

The direction (orientation) of the tropopause fold object is critically important. The final step in Table 2 limits the areas of interest to those that are normally aligned with a strong jet stream ($>330^\circ$ or $<120^\circ$). Furthermore, a pair of output fields defines the two directions of flight that would be the most prone to turbulence, because the turbulence takes the form of eddies whose rotational axes align with the flow, and therefore have an anisotropic effect on the disturbances experienced by aircraft passing through the tropopause folds (Figure 14).

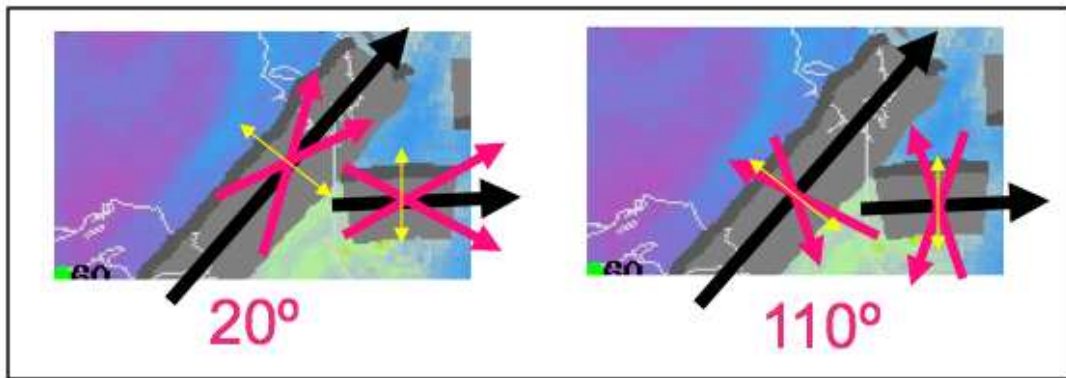


Figure 14. Examples of flight direction relative to the tropopause fold. Left: Flight directions crossing tropopause folds at 20° . Right: Flight directions crossing at 110° . The black arrows are the orientations of the tropopause folds. The “caution directions” of the larger and smaller tropopause folds are perpendicular to the black arrow: 315° , 135° for the larger; and 0° , 180° for the smaller (yellow vectors).

Finally, the remaining tropopause folds are situated vertically. The middle height at the side of the tropopause break is the height of the tropopause on the colder side of the boundary. The opposite end is a height lower by 5K (potential temperature). The method for this height assignment is presented in Figure 15. (This matches the relative location of the tropopause fold depicted in the idealized cross section in Figure 16.) The upper and lower bounds of this volume are at 5K (potential temperature) above and below this middle height across the tropopause fold.

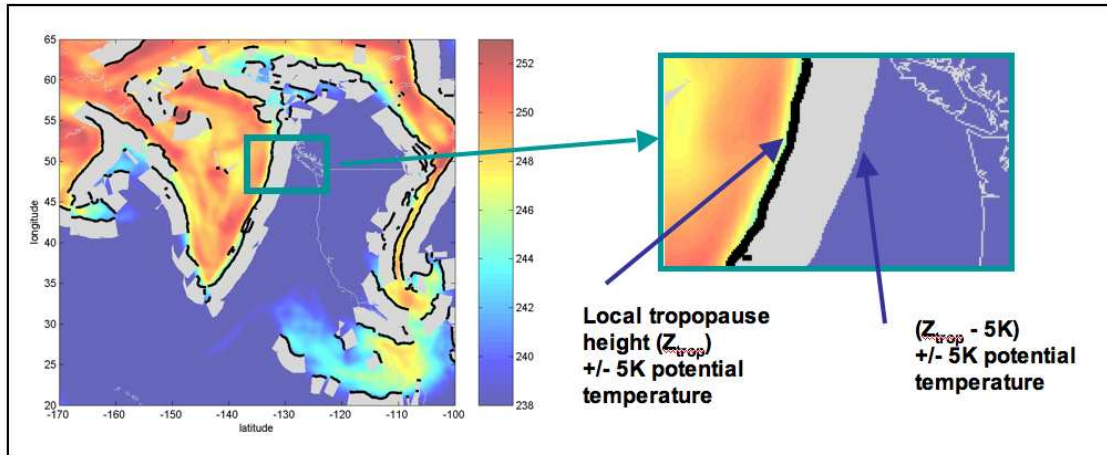


Figure 15. Height assignment of the tropopause folds.

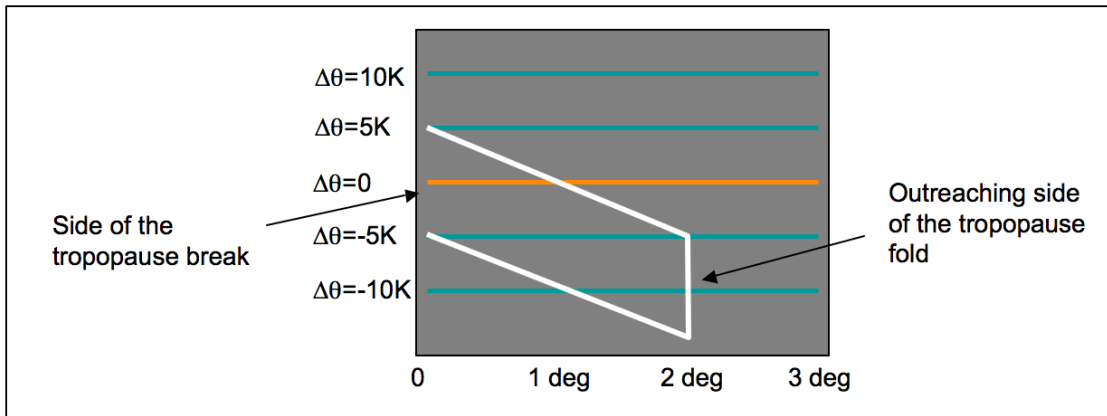


Figure 16. Cross-sectional depiction of the tropopause fold height assignment.

3.4.3 Algorithm Output

The final output of this algorithm is a “mask” of turbulence direction and height, in addition to a quality flag field. These variables and a description of their meaning are given below (Table 3).

Table 3. TFTP output products.

| Product field | Data type | Description |
|------------------|-------------|---|
| Lowermost height | 4-byte real | Lower height of the turbulent tropopause fold volume. |

| | | | |
|----------------------|----------------|--|---|
| Uppermost height | 4-byte real | Upper height of the turbulent tropopause fold volume. | |
| Caution direction #1 | 4-byte real | Direction of flight (0-360°) in which an aircraft is susceptible to turbulence | |
| Caution direction #2 | 4-byte real | Other susceptible direction, 180 degrees from Caution direction #1 | |
| Quality flags | 1-byte integer | Bit 0 | Zenith angle quantitative product domain (0: OK, 1: LZA >70°) |
| | | Bit 1 | Satellite brightness temperature quality (0: OK, 1: bad data) |
| | | Bit 2-7 | Not used |
| Quality check | 1-byte integer | Bit 0 | Output fields quality indicator (0: OK, 1: bad data) |
| | | Bit 1-7 | Not used |

The first two output products constrain the tropopause folds in space. The horizontal distribution of the tropopause folds is defined by the location of non-missing values. All other pixels without tropopause folds receive missing values. The vertical distribution is then defined by the location between the lowermost and uppermost height. Next, the second two output products define the two directions of flight that are the most prone to experiencing turbulence, because turbulent eddies near the jet are an anisotropic phenomenon.

The quality flag output is a single byte using two bits to indicate the zone of the product within the zenith angle domain and the coverage of good data. The quality check output indicates the goodness of the output data.

The algorithm also supplies a set of metadata output fields, as 4-byte real scalars, to serve for diagnostic and statistical purposes (Table 4).

Table 4. *TFTP Metadata output.*

| Variable | Description |
|-----------------|---|
| TF pre-count | Number of initial tropopause fold objects |
| TF post-count | Number of final tropopause fold objects |

| | |
|-----------|--|
| Z_lo min | Minimum value of tropopause fold lowermost heights in product |
| Z_lo max | Maximum value of tropopause fold lowermost heights in product |
| Z_lo mean | Average value of tropopause fold lowermost heights in product |
| Z_lo std | Standard deviation of tropopause fold lowermost heights in product |
| Z_hi min | Minimum value of tropopause fold uppermost heights in product |
| Z_hi max | Maximum value of tropopause fold uppermost heights in product |
| Z_hi mean | Average value of tropopause fold uppermost heights in product |
| Z_hi std | Standard deviation of tropopause fold uppermost heights in product |

4.0 TEST DATA SETS AND OUTPUTS

4.1 Simulated Input Data Sets

The following input data is used to characterize the performance of the algorithm and the quality of the data products.

4.1.1 GOES-12 water vapor imagery

GOES-12 water vapor imagery (channel 3, $6.3\mu\text{m}$) is used as a proxy for ABI channel 8 ($6.15\mu\text{m}$) water vapor channel. The most significant difference expected between these two channels is a small offset in brightness temperature due to their slightly different contribution weighting function heights. However, an offset value makes no difference in the image spatial gradient, which is the key calculation in resolving the boundaries used to calculate tropopause folds. Differences in spatial resolution are also unimportant, because the algorithm image-smoothing function retains only the features at a scale of ~ 66 km or larger. Thus, the GOES-12 channel 3 data source is a natural proxy for testing the algorithm performance.

For algorithm validation, the GOES-12 Northern Hemisphere scan sector is used (Figures 17, 18)

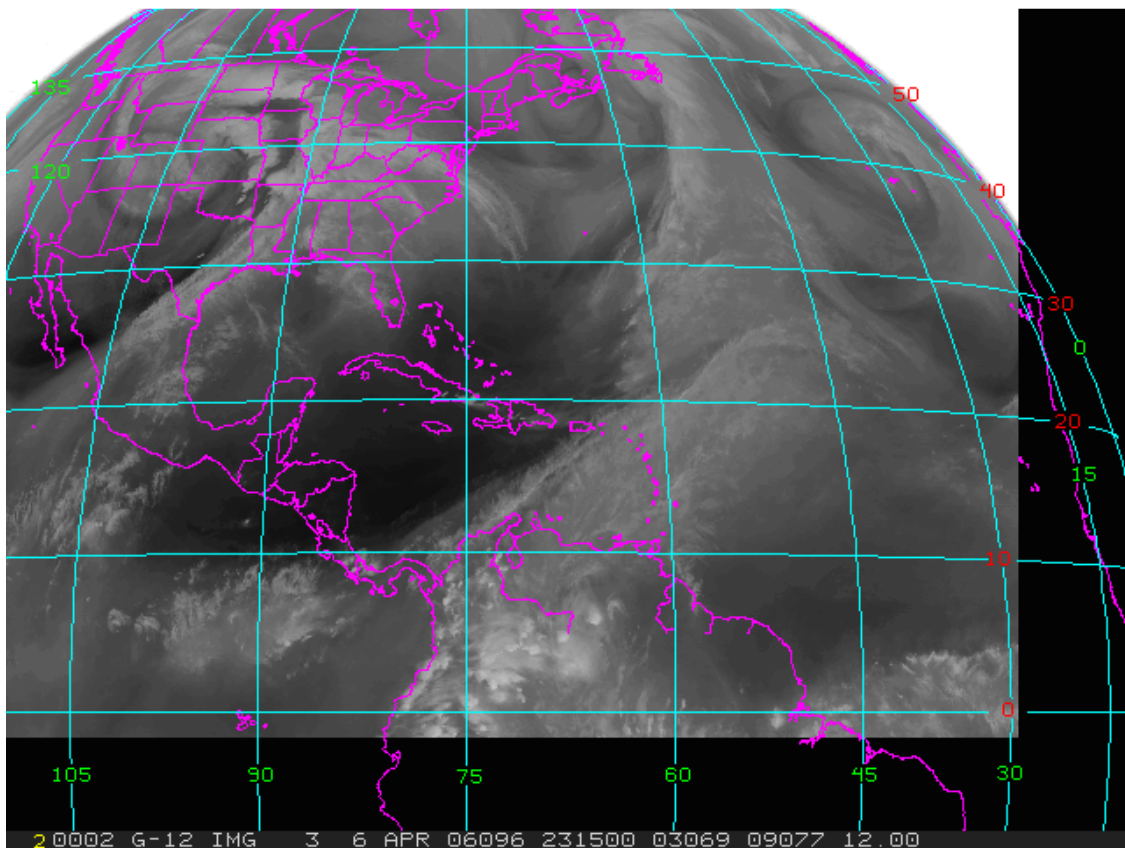


Figure 17. Domain of the input data sets, using GOES-12 water vapor archived imagery. This example is for 6 April 2006 2345 UTC.

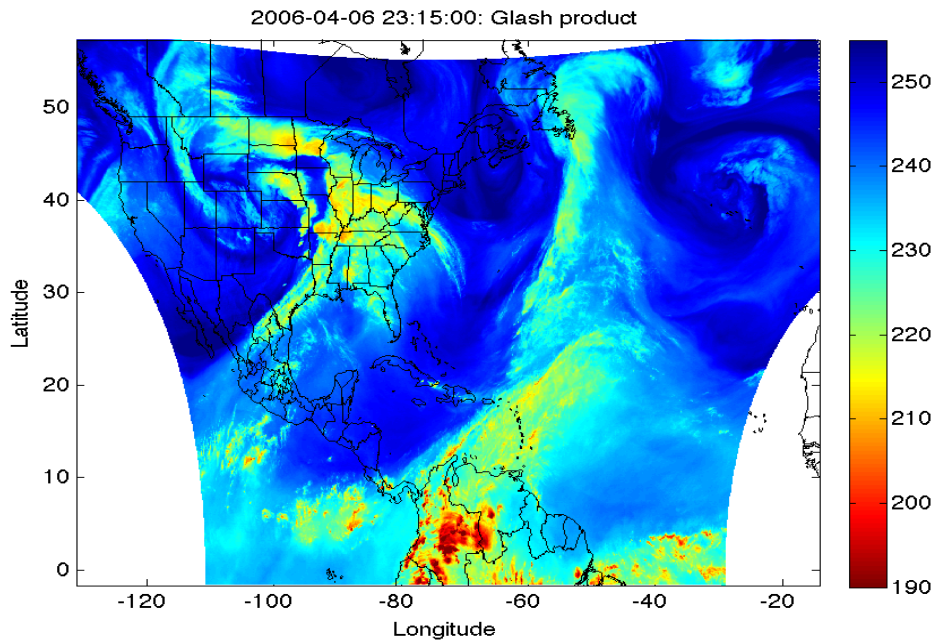


Figure 18. GLASH product corresponding to the previous figure to show the input domain in the rectilinear coordinates used in subsequent figures.

4.1.2 GFS forecast model fields

Ancillary model fields are supplied by the GFS forecast model. Gridded fields are global with 1-degree resolution. The 12-hour forecast at 6-hour resolution is used to simulate the best available forecast fields in real time. Model values at the exact time of the image are calculated through temporal interpolation.

4.1.3 Test data set sample

The following ten cases are presented in the delivery of this document for independent verification of algorithm performance (Table 5). These cases were not chosen randomly but rather, they were found to have some of the most abundant corresponding independent verification data in order to illustrate the verification process the most easily.

Table 5. Times of the sample images for the initial verification.

Sample image time

-
1. 2005 Dec 22 1715 UTC
 2. 2005 Dec 22 2015
 3. 2006 Apr 06 2315
 4. 2006 Apr 15 2315
 5. 2006 Sep 21 1715
 6. 2007 Jan 04 2315
 7. 2007 Mar 29 2015
 8. 2007 Mar 29 2315
 9. 2007 Jun 06 2315
 10. 2007 Dec 03 2015

4.2 Output from Simulated Input Data Sets

This section characterizes the output data in terms of its precision, accuracy and error budget. An example of the output produced by the input image from Section 4.1 is shown below for reference (Figure 19).

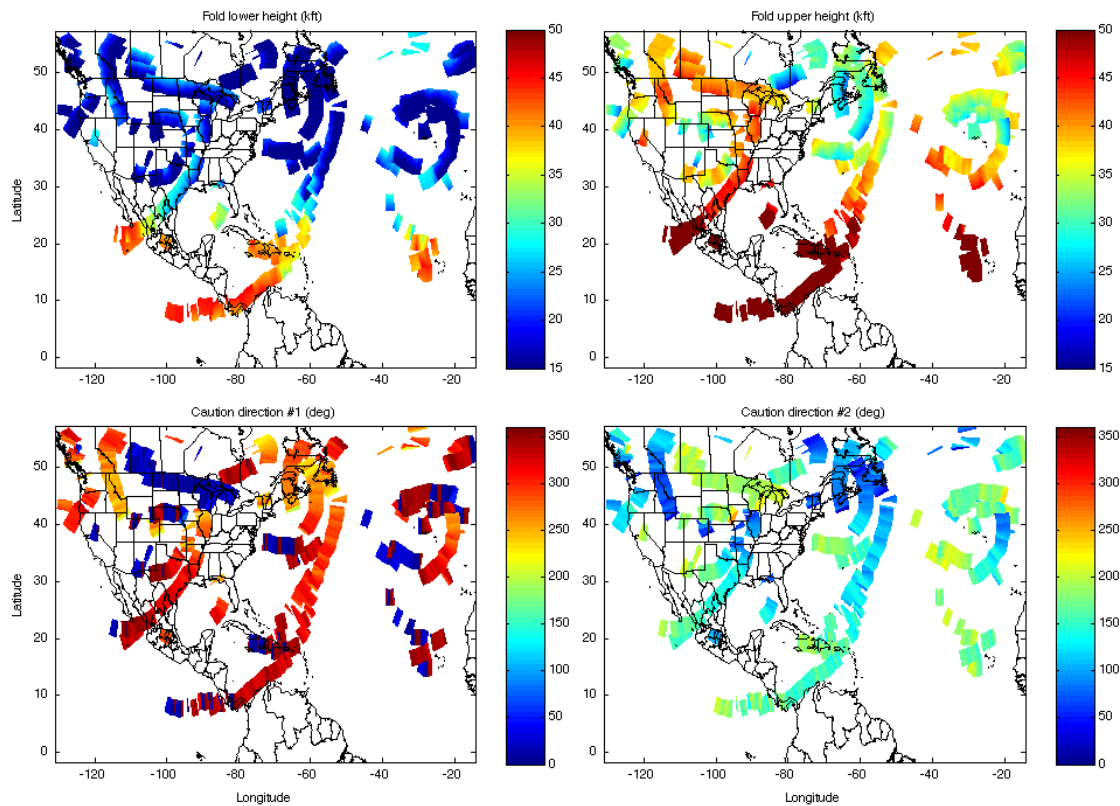


Figure 19. TFTP output products for 6 April 2006 2345 UTC. Upper-left: Fold lower height (kft); Upper-right: Fold upper height (kft), Lower-left: Caution direction #1 (degrees); Lower-right: Caution direction #2 (degrees).

In these products, the colored regions are identified as areas of tropopause folds, and the white space is the remaining area, which is assigned a pixel value of “Missing.”

4.2.1 Precisions and Accuracy Estimates

Precision and accuracy relate to the TFTP product in three ways – horizontal, vertical and directional. Horizontal precision and accuracy affect all four TFTP output fields in the same way. Vertical precision and accuracy concern the first two TFTP output fields, which constrain the height of the regions of interest. Finally, directional precision and accuracy concern the values of the remaining two output fields of “caution direction.” The precision and accuracy of these products are summarized in Table 6 and described in the following subsections. Note that precision and accuracy relate to the position of the tropopause fold volume. The predictability of the relationship between tropopause folds and turbulence is handled by the Error Budget (Section 4.2.2).

Table 6. Summary of the sources of output precision and accuracy.

| Output parameter | Value | Primary dependence |
|-------------------------|--------------|--|
| Horizontal precision | 0.25 km | ABI horizontal precision |
| Horizontal accuracy | 1 km | ABI horizontal accuracy |
| Vertical precision | < 1m | GFS tropopause height precision |
| Vertical accuracy | 2 km | GFS tropopause height accuracy at forecast time of 12 hours |
| Directional precision | < 0.1° | Precision of smoothed gradient contours |
| Directional accuracy | < 10° | Perturbations in contour position from small-scale boundary features |

4.2.1.1 Horizontal Precision

The TFTP product operates at the resolution and the navigation of the input satellite imagery, which means that it shares the horizontal precision of the input satellite imagery. For ABI input, the TFTP shares the ABI product horizontal precision of 0.25 km. (This number is based on the overlap and spacing of the 2-km resolution ABI pixel.)

4.2.1.2 Horizontal Accuracy

As opposed to products with pixel-based retrievals of atmospheric constituents, the TFTP is effectively insensitive to the systematic error of the ABI brightness temperatures when the ABI brightness temperatures are within the product requirements. This is because the product relies on 1) a large (~66 km) averaging filter; and 2) gradient calculations that eliminate the effect of brightness temperature bias. The only remaining effect of ABI error on the TFTP horizontal accuracy is the spatial navigation. A systematic bias in spatial positioning will carry over into the spatial precision of the product. Thus the horizontal accuracy of the product is the same as the ABI product requirement of 1 km (Gibbs, 2008).

4.2.1.3 Vertical Precision

Vertical positioning is determined by the tropopause height of the ancillary atmospheric model and the potential temperature heights. The precision of these values is less than a meter in the vertical dimension, which is more precise than that of any independent validation.

4.2.1.4 Vertical Accuracy

The GFS tropopause height comes directly from the WMO definition of the thermal tropopause: It is defined as the lowest level at which the lapse rate decreases to 2 °C km⁻¹ or less, provided that the average lapse rate between this level and all higher levels within 2 km does not exceed 2 K km⁻¹ (WMO, 1957). GFS documentation does not quantify the accuracy of the tropopause height at either the analysis or forecast time. However, we can estimate that the largest source of variance in the tropopause height in the 12-hour GFS forecast is the displacement of real and forecast boundaries around the upper-air front, and a rough estimate of that value based on inspection of a representative sample of TFTP applications is approximately 2 km. The vertical accuracy of tropopause height will certainly affect the performance of the TFTP product, and this is evaluated in the product validation (Sections 4.2.2 and 5.5).

4.2.1.5 Directional Precision

The precision of the caution direction is less than a tenth of a degree. This value depends directly on the precision of the contours, which is highly precise because of the large spatial averaging filter (>60 km) applied to the imagery being contoured.

4.2.1.6 Directional Accuracy

The departure between the intended direction and the direction depicted in the product is primarily due to the effect of small perturbations in the contour position, which magnifies in the final analysis of feature direction. Inspection of a sample of cases reveals that this leads to a directional accuracy of approximately 10 degrees or less. A more thorough analysis would not be productive because the only valid evaluation of this output field's viability is the product validation (Sections 4.2.2 and 5.5).

4.2.2 Error Budget

The product performance is evaluated against independent measurements of moderate or greater (MOG) turbulence near the nominal time of the image. The methodology used here is described in detail in the Algorithm Validation in Section 5.5.

Independent measurements of MOG turbulence are collected in one-minute samples on commercial aircraft of Eddy Dissipation Rate (EDR). In the product validation we use collocated EDR within one hour before or after the nominal time of the output product. To illustrate one example, the distribution of in-situ Eddy Dissipation Rate (EDR) is seen to intersect some of the tropopause folds (Figure 20).

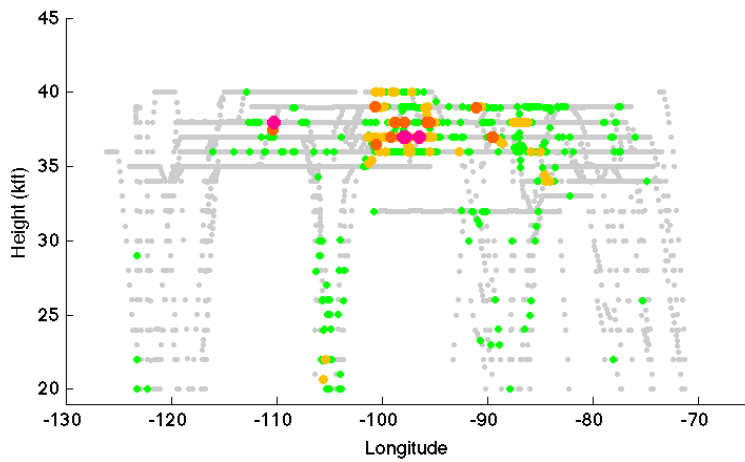
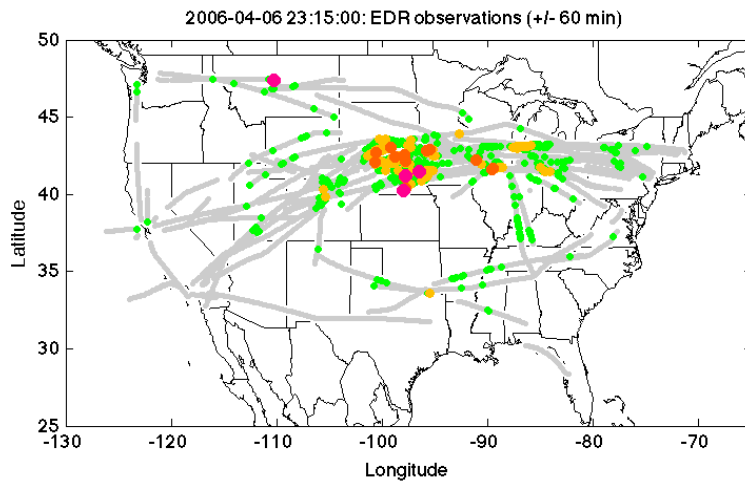


Figure 20. In-situ validation data for 6 April 2006 2315 UTC; MOG turbulence observations are “hot” colors – yellow, orange and red; light turbulence is green and null values are gray. Top: Horizontal distribution; bottom: Vertical distribution.

We further limit the sample of EDR values to the points that sit within the tropopause fold volume and within the range of valid flight directions affected by tropopause fold turbulence (Figure 21).

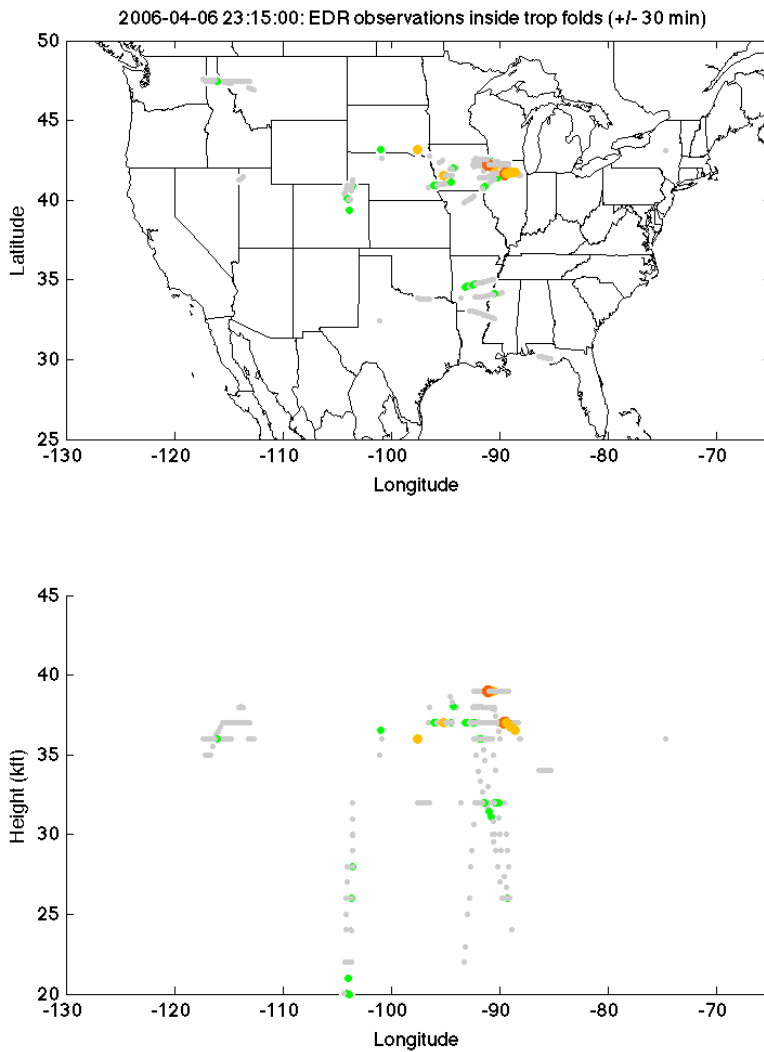


Figure 21. As in Figure 17, but limited to the volume and direction of the predicted tropopause folds.

These data points are used in the product validation as follows. The TFTP accuracy requirement is defined as “50% correct detection of Moderate or Greater turbulence” calculated as

$$f = 1 - (1 - p)^{16} \quad (10)$$

where f is the probability of a turbulent event at the spatial scale of tropopause folds (200 km), p is the fraction of MOG events to the total number of measurements in the regimes

of output tropopause folds and the exponent is a scaling factor. This formula is derived in Section 5.5.

We arrive at the error budget for the TFTP product by calculating this formula for all the points in the validation sample. In the current iteration of the calculation, we use the images from the data delivery with this version of the ATBD to arrive at the TFTP measurement accuracy of 46%, which meets the 80% requirement for the Version 3 delivery (Table 7).

Table 7. Results of the most recent TFTP validation.

| # Total measurements in trop. folds | # MOG events | Probability of MOG at the spatial scale of trop. folds | Product requirement |
|--|---------------------|---|----------------------------|
| 2364 | 88 | 46% | 50% |

This current error budget is limited in scope and subject to several major changes before the next ATBD delivery, although it does provide an important framework for further discussion and assessment. The future error budget will come from a validation to be completed in October 2010 using 1125 images.

In addition, the TFTP product is subject to future changes to improve its accuracy, especially in the vertical dimension. In order to increase the measurement accuracy and meet or exceed the 50% standard, the TFTP can be adjusted with stricter thresholds, most notably the brightness temperature gradient thresholds, or the limits of the tropopause fold directional range. The optimum adjustments will be determined through an error analysis that isolates the probability of MOG turbulence with respect to the height relative to the tropopause, the gradient magnitude at the boundary and the relative flight direction.

5.0 PRACTICAL CONSIDERATIONS

5.1 Numerical Computation Considerations

The algorithm takes a satellite image as either an entire data field, or as two data fields for the northern and southern hemispheres. This contrasts with the more common technique in other GOES-R algorithms that input only a few scan lines per operation.

Because of the image-wide operations in the algorithm, the TFTP requires several large two-dimensional arrays that are assigned in Fortran to the heap memory space (using the `ALLOCATE` and `DEALLOCATE` functions). This has not overburdened the platforms running the algorithm in test mode, but it is a distinguishing feature nonetheless.

It is also important to limit the input ancillary model levels to between only 50 hPa and 700 hPa (a reasonable range for the location of tropopause folds) to save memory.

The navigation, sampling and interpolation procedures assume a rectilinear grid for the ancillary model information.

5.2 Programming and Procedural Considerations

The TFTP algorithm uses the following third-party subroutines in its operation. They have been altered as little as possible from their original state in order that their documentation or user community knowledge may still apply to the code, and therefore some aspects of these subroutines do not conform to the AWG coding standards:

- **Subroutine ValueToGrid:** Interpolates data from one mesh-style projection into another. Each output grid cell is matched to a surrounding quadrilateral in the input grid, found through an iterative search. The value in the output grid cell is calculated from three points on the matching input grid quadrilateral by reverse interpolation. This subroutine originated as a Java remapping algorithm for McIDAS-V software developed at CIMSS.
- **Subroutine TWMO:** Calculates the WMO-defined tropopause height from an input model grid when the model does not have a pre-calculated tropopause. The algorithm is presented in Reichler et al. (2003).
- **Subroutine QSORTI:** Popular quick sorting algorithm for integer input arrays with a forty-year heritage.
- **Subroutine UsgsContour:** Contouring algorithm shared by the U.S. Geological Survey (Harbaugh, 1990). This takes a two-dimensional real array and returns line segments at the desired contour levels. In our implementation, the desired contour level is always zero. Contours are developed through an iterative search of neighboring grid cells and interpolation.

5.3 Quality Assessment and Diagnostics

We recommend that the product be evaluated post-hoc with aircraft EDR data on seasonal and yearly intervals. The robustness of the validation should steadily improve with time as more airlines volunteer to participate in automated in-situ monitoring and increase the spatial domain of the in-situ data set.

5.4 Exception Handling

Missing input imagery or ancillary model fields will cause an exception and exit processing. Also, incorrectly navigated imagery will cause an error in the memory allocation of intermediate processing grids and exit processing. Otherwise, the algorithm will process the output under any conditions and produce error flags where the output is adversely affected by bad input pixels (Section 3.4.3).

5.5 Algorithm Validation

5.5.1 Validation activities

The pre-AWG validation of the TFTP algorithm focused on predicting Light or Greater (LOG) turbulence (Figure 7), but a 2009 change in the product requirements nullified this validation by specifying that the performance predict MOG turbulence. A validation to address this requirement has been scheduled, with a 1 October 2010 completion date. The input data set (GOES-12 imagery and ancillary model fields) was prepared and delivered at the end of March 2010.

The new validation data set consists of 1125 images from 1415, 1715, 2015 and 2315 UTC during the days between 1 November 2005 and 28 February 2008. These times coincide with the times of day with the most commercial aircraft activity and therefore the highest density of independent in-situ data. The individual days in the data set from which the images are taken are spaced three days apart to insure the observation of separate synoptic weather events. With this volume of data we expect to be able to analyze $\sim 10^5$ data points inside the tropopause fold domain.

5.5.2 Independent validation data set

The independent validation data is in-flight, automated observations by small instruments carried on commercial aircraft. The variance in the measured wind field is processed and recorded as “Eddy Dissipation Rate,” (EDR) (Cornman et al., 2004). These data are bundled with other observations (air temperature, pressure, etc.) as averages and min/max values over one-minute segments and broadcast to ground stations, where they are subsequently quality-controlled and used for meteorological applications. In the case of turbulence, the relevant quantity is the maximum EDR value over the time segment. The position of the data is the position of the aircraft in the middle of the one-minute flight segment.

By convention, EDR values of 0.25 and higher are MOG turbulence, whereas 0.05 is null and 0.15 is light turbulence. This differs slightly from the threshold of 0.35 for MOG used in other studies, because those studies use the 737 and 757 aircraft as the baseline for the experience of turbulence. However, the most dangerous events on record occur with lighter aircraft, which experience turbulence at a lower equivalent EDR.

5.5.3 Validation strategy

The following section describes the derivation of the accuracy statistic using EDR data.

5.5.3.1 Rationale

The independent EDR data set records the maximum turbulence observed at a temporal resolution of one minute. A previous validation that considered the performance of the TFTP at this resolution found a product accuracy of 20% for Light or Greater turbulence and 5% for Moderate or Greater turbulence, as reported in the Algorithm Theoretical Basis Document (ATDB) Version 1.0. However, we are not able to calculate accuracy in the manner similar to most of the other ABI products. The standard measure of accuracy for ABI products, by the convention of the Atmosphere-Ocean-Land Technical Advisory Panel (AOL-TAP), is:

$$\text{Accuracy} = (\text{YY} + \text{NN}) / (\text{YY} + \text{YN} + \text{NY} + \text{NN}) \quad (11)$$

where “YN” indicates a positive prediction and negative observation, “NY” indicates a negative prediction and positive observation, and so on.

However, the TFTP only produces a set of regions in which one source of turbulence is expected. (It does not make a prediction on the location of turbulence caused by mountain waves, convective gravity waves, etc.) That is, the TFTP only makes positive predictions, but the regions without a prediction are not necessarily negative predictions. Thus we must measure the accuracy as

$$\text{Accuracy (for TFTP)} = (\text{YY}) / (\text{YY} + \text{YN}). \quad (12)$$

One should expect this measure of accuracy to be lower than that of the first option, because turbulence is much less common than stable air in the upper atmosphere. Thus, if we were able to use the first method, “NN” would dominate. This means that any value for accuracy using the second method would be comparable to a much higher value using the first method, assuming both were able to be calculated.

5.5.3.2 Applying an accuracy statistic on tropopause folds

The TFTP predicts regions of active tropopause folds. We note, however, that these features are not constantly turbulent. Rather, they prescribe a region in which short-lived, transient eddies are generated over a fraction of their total volume. Our overall goal is not to describe exactly where and when each turbulent eddy can be found, but rather to

describe the region in which an aircraft should show extra caution, either by modifying flight plans or by warning passengers and crew to remain seated and secured.

We validate the TFTP by identifying the thousands of observations that fall within the volumes of predicted turbulence (inside the ribbon-shaped tropopause folds of the satellite product and between the upper and lower altitude bounds). To calculate a simple fraction of turbulent observations would be to address the question, “What is the likelihood of turbulence during a one-minute flight segment in this region of interest?” This may be the most direct use of the validation data, but it stems from an arbitrary integration time that does not match the assumptions and expectations of the aviation community.

By contrast, a more natural question that we should attempt to address would be, “What is the likelihood of turbulence during the course of a transect through this tropopause fold?” As the following illustration shows, the scale of the region of interest is equivalent to *many* one-minute validation segments (Figure 22). Also, this illustration shows how a longer integration time leads to an arbitrarily higher number for the product’s accuracy.

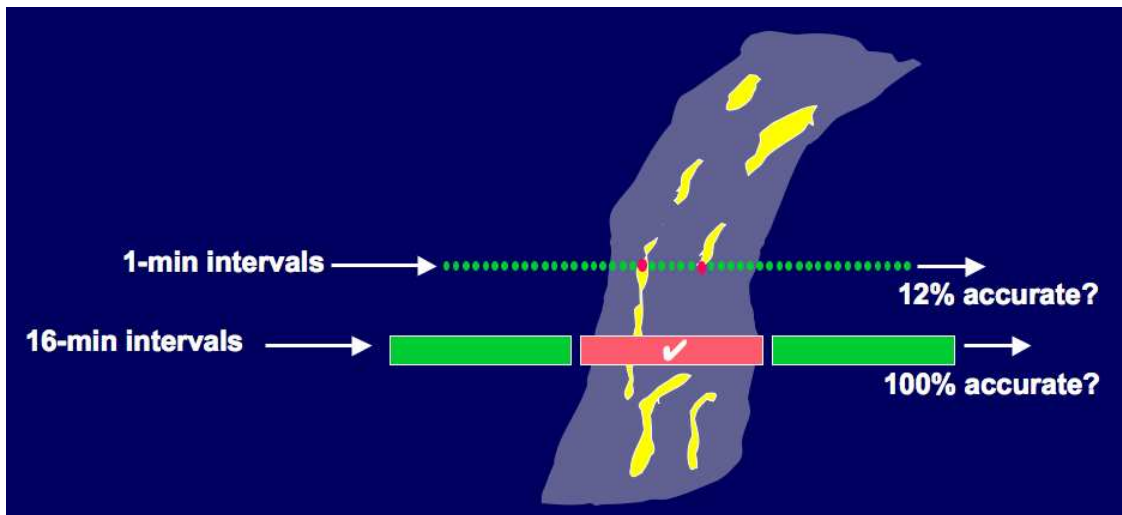


Figure 22. Conceptual diagram of two aircraft passes through a tropopause fold, scaled to the average width of a tropopause fold (shown in gray) and the typical speed of a commercial jet passing through. Areas of short-lived atmospheric instability are shown in yellow. Green segments are “no turbulence” reports and red segments are turbulent reports. The top pass supposes a one-minute interval between observations, and the bottom pass supposes a 16-minute interval between observations.

5.5.3.3 Normalizing the EDR observations to the appropriate scale

Because of the anisotropic nature of turbulence caused by tropopause folding, the product predicts turbulence only in cases in which the aircraft crosses the ribbon-like tropopause fold feature orthogonally (an incident angle of +/- 20 degrees). In the product, these

features are always a fixed width (200 km). Thus, the average time in which an aircraft would transect a tropopause fold (assuming it does not cross just a piece of it) would be

$$T = 200 \text{ km} / R \quad (13)$$

where T is the length of time for a full transect and R is the aircraft speed. An average commercial aircraft's cruising speed is about 460 knots, or 740 km/hr. Thus according to the formula an average transect time would be .27 hours, or 16 minutes.

This result corresponds to sixteen sequential observations. Assuming independent observations, the likelihood of experiencing at least one turbulent episode over sixteen one-minute time segments is:

$$f = 1 - (1 - p)^{16} \quad (\text{Equation 10})$$

where p is the probability of detecting turbulence over a one-minute interval. When $p = 5\%$ as have found in the original validation for Moderate or Greater turbulence, then $f = \underline{56\%}$. This statistic (Equation 10) is used to compare the product performance to the performance requirement.

6.0 ASSUMPTIONS AND LIMITATIONS

The following sections describe the current limitations and assumptions in the current version of the TFTP.

6.1 Performance

The following assumptions have been made in developing and estimating the performance of the TFTP. The following short list contains the current assumptions and proposed mitigation strategies.

1. NWP data of comparable or superior quality to the current 6 hourly GFS forecasts are available. (Mitigation: Use longer range GFS forecasts or switch to another NWP source such as ECMWF.)
2. Hourly temperature and tropopause break heights are well approximated by interpolating the NWP data, assumed to be 6-hourly or better. (Mitigation: Use the internal tropopause height algorithm.)
3. EDR reports have been quality-checked by NCAR. (No mitigation possible.)

6.2 Assumed Sensor Performance

We assume the sensor will meet its current specifications. However, the TFTP will be dependent on the following instrumental characteristics.

- Severe striping in ABI channel 8 (sufficient to pass through the spatial filter) will prevent a product calculation in a wide band around the stripes of bad pixels.
- Errors in navigation from image to image will create a corresponding displacement in the product features. Severe navigation errors will throw an exception and terminate the algorithm.

6.3 Pre-Planned Product Improvements

6.3.1 Optimization for Ocean Domain

At present, the EDR reports are not available over the ocean and so the parameterization of the TFTP was performed over land only. However, we have reason to believe that the TFTP would have a slightly different set of parameterizations over the ocean because of the smoother texture of the water vapor channel in that domain. When NCAR receives access to EDR reports over the ocean, we recommend making a separate optimization over the ocean.

6.3.2 Limitations of the Algorithm

The following limitations have been discussed in previous sections:

- We have determined that significant clear-air turbulence events caused by tropopause folding in the months of May to October are comparatively rare, and so these events will not be predicted as often by the TFTP.
- The height assignment of tropopause folds is dependent on the model-determined tropopause height.

7.0 REFERENCES

- Browell, E.V. et al. (2003), Ozone, aerosol, potential vorticity, and trace gas trends observed at high-latitudes over North America from February to May 2000, *J. Geophys. Res.*, **108**(D4).
- Cho, J. Y. N., et al. (1999), Observations of convective and dynamical instabilities in tropopause folds and their contribution to stratosphere-troposphere exchange, *J. Geophys. Res.*, *104*, 21,549-21,568, 1999.
- Cornman, L. B., P. Schaffner, C. A. Grainger, R. T. Neece, T. S. Daniels and J. J. Murray (2004), Eddy dissipation rate performance of the Tropospheric Airborne Meteorological Data Reporting (TAMDAR) sensor during the 2003 Atlantic THORPEX regional campaign, AMS 11th conference on aviation, range and aerospace.
- Danielson, E. F. (1968), Stratospheric-tropospheric exchange based on radioactivity, ozone and potential vorticity. *J. Atmos. Sci.* *25*, 502- 518.
- Gibbs, B. (2008) GOES image navigation and registration, *SatMagazine*, July 2008 Edition, http://www.satmagazine.com/cgi-bin/display_article.cgi?number=1889485593.
- Harbaugh, A.W., 1990, A simple contouring program for gridded data: U.S. Geological Survey Open-File Report 90-144, 37 p.
- Holton, J.R., P.H. Haynes, M.E. McIntyre, A.R. Douglass, R.B. Rood, and L. Pfister (1995), Stratosphere-Troposphere Exchange, *Rev. Geophys.*, *33* (4), 403-439.
- Johnson, W.B., and W. Viezee (1981), Stratospheric ozone in the lower troposphere--I. Presentation and interpretation of aircraft measurements, *Atmos. Environ.*, *15* (7), 1309-1323.
- Keyser, D., and M. J. Pecnick, (1985a), A two-dimensional primitive equation model of frontogenesis forced by confluence and horizontal shear. *J. Atmos. Sci.*, *42*, 1259-1282.
- Keyser, D., and M. J. Pecnick, (1985b), A review of the structure and dynamics of upper-level frontal zones. *J. Atmos. Sci.*, *42*, 1283-1305.
- Keyser, D. and M. A. Shapiro (1986), A review of the structure and dynamics of upper-level frontal zones. *Mon. Wea. Rev.*, *114*, 452-499.
- Marroquin, A. (1998), An advanced algorithm to diagnose atmospheric turbulence using numerical model output. Preprints, 16th Conf. on Weather Analysis and Forecasting, Phoenix, AZ, Amer. Meteor. Soc., 79-81.

- Reeder, M. J., and D. Keyser, (1988), Balanced and unbalanced upper-level frontogenesis. *J. Atmos. Sci.*, 45, 3366-3386.
- Reichler, T., M. Dameris, and R. Sausen (2003), Determining the tropopause height from gridded data, *Geophys. Res. Lett.*, 30(20), 2042, doi:10.1029/2003GL018240.
- Shapiro, M.A. (1980), Turbulent mixing within tropopause folds as a mechanism for the exchange of chemical constituents between the stratosphere and troposphere, *J. Atmos. Sci.*, **37**, 994-1004.
- Shapiro, M.A. (1981), Frontogenesis and geostrophically forced secondary circulations in the vicinity of jet stream-frontal zone systems, *J. Atmos. Sci.*, **38**, 954-973.
- Shapiro, M. A., and D. Keyser (1990), Fronts, jet streams and the tropopause. *Extratropical Cyclones, The Erik Palmén Memorial Volume*, C. W. Newton and E. O. Holopainen, Eds., Amer. Meteor. Soc., 167-191.
- Wimmers, A.J., and J.L. Moody (2001), A fixed-layer estimation of upper tropospheric specific humidity from the GOES water vapor channel: Parameterization and validation of the altered brightness temperature product, *J. Geophys. Res.*, **106** (D15), pp 17115-17132.
- Wimmers, A. J., and J. L. Moody (2004a), Tropopause folding at satellite-observed spatial gradients: 1. Verification of an empirical relationship, *J. Geophys. Res.*, **109**, D19306, doi:10.1029/2003JD004145.
- Wimmers, A. J., and J. L. Moody (2004b), Tropopause folding at satellite-observed spatial gradients: 2. Development of an empirical model, *J. Geophys. Res.*, **109**, D19307, doi:10.1029/2003JD004146.
- Wimmers, A. J., C. Schmidt, W. Feltz, and J. R. Mecikalski (2004) Satellite Applications for Detection of Atmospheric Turbulence Related to Tropopause Folding, AMS 11th conference on aviation, range and aerospace.
- Wimmers. A. J. and W. Feltz (2005) Estimating regions of tropopause folding and clear-air turbulence with the GOES water vapor channel, World Research Symposium on Nowcasting and Very Short Range Forecasting.
- World Meteorological Organization (1957), Definition of the tropopause, *World Meteorological Organization Bull.* 6, 136.